Analysis of shingle interconnections in solar modules by scanning acoustic microscopy

Cite as: AIP Conference Proceedings **2147**, 090003 (2019); https://doi.org/10.1063/1.5123871
Published Online: 27 August 2019

Laila Veríssimo Mesquita, Nils Klasen, Esther Fokuhl, Daniel Philipp, and Luciana Pitta Bauermann

Analysis of Shingle Interconnections in Solar Modules by Scanning Acoustic Microscopy

Laila Veríssimo Mesquita[a)], Nils Klasen, Esther Fokuhl, Daniel Philipp, Luciana Pitta Bauermann

Fraunhofer Institute for Solar Energy Systems ISE, Heidenhofstrasse 2, 79110 Freiburg im Breisgau, Germany

[a)]Corresponding author: laila.verissimo.mesquita@ise.fraunhofer.de

Abstract. Scanning Acoustic Microscopy (SAM) is applied as a non-destructive testing to image the electrically conductive adhesive (ECA) joints used to connect shingled solar cells. The advantage of SAM is the possibility of imaging the internal structure of the material, which enables the visualization of the depth profile. In this work, we demonstrate the suitability of SAM for detecting ECA failures in shingled cells that are embedded within a solar module. Shingled interconnected cells were prepared by intentionally applying ECA strips equally spaced apart between adjacent cells. Single acoustic images from different layers inside shingle modules were obtained, as well as acoustic cross-sections. X-ray imaging was carried out to compare with the images obtained by SAM. Additionally, Electroluminescence imaging was further carried out to compare the electrical performance of the shingled cells with the physical distribution of the ECA joints. The results reveal that SAM is capable of imaging the structure of the ECA inside solar modules, and distinguishing intact ECA from defective adhesive areas. Therefore, SAM can be applied as a complementary technique to the qualitative analysis of ECA joints.

INTRODUCTION

Acoustic Microscopy is a non-destructive testing (NDT) method whose working principle lies in the detection of reflected acoustic waves at interfaces of materials with different acoustic properties, i.e., acoustic impedances [1]. Acoustic waves are sensitive to interfaces and material discontinuities, besides enabling the investigation of opaque and transparent materials [2]. Here, the Scanning Acoustic Microscopy (SAM) is considered as an NDT to assess qualitatively the application process of electrically conductive adhesive (ECA) used in shingled interconnections in solar modules by detecting failures, such as voids, material disruption, and flaws.

In shingle modules, the rear and front sides of two adjacent strip-like solar cells overlap, and their connection is established by soldering or applying ECA. The latter consists of an organic matrix with uniformly distributed electrically conductive particles. In a shingled arrangement, the front and rear side busbars are covered, and no cell spacing is present in the module, as shown in Fig. 1 [3,4,5]. Connecting the cells directly via ECA is advantageous because it eliminates the need for front-to-back interconnect ribbons, therefore reducing ohmic losses. Nevertheless, applying ECA comes at the cost of fulfilling additional mechanical needs to cover for the thermomechanical stresses at the overlap areas between the brittle cells [5,6]. Interconnection failure may arise because of ECA deformation upon different mechanical responses of the materials due to varying external stresses [5]. Therefore, studying the physical distribution of ECA is crucial to detect defective adhesive areas and understand likely failure development on shingle modules.

Our approach focuses on the application of SAM to study the quality of ECA. X-ray imaging was carried out to compare with the results obtained. X-ray imaging enables the visual inspection of internal layers of objects with complex morphologies non-destructively; therefore, it is used as a reference technique [7,8]. Besides, Electroluminescence (EL) imaging of the single modules was carried out to validate the information acquired by SAM. EL is a standard method used to provide reliable information on cell interconnection defects, and, in this case, on the integrity of the electrical contact between the cells.

SiliconPV 2019, the 9th International Conference on Crystalline Silicon Photovoltaics
AIP Conf. Proc. 2147, 090003-1–090003-8; https://doi.org/10.1063/1.5123871
Published by AIP Publishing. 978-0-7354-1892-9/$30.00

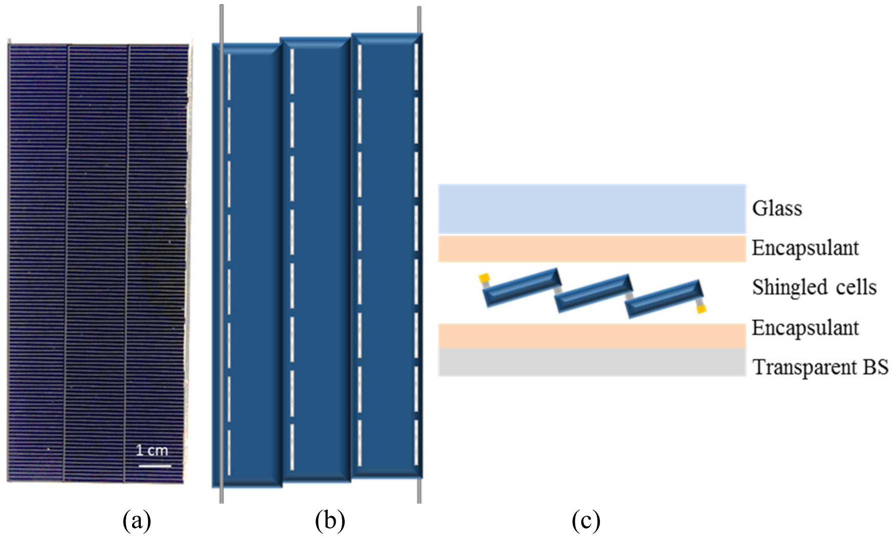

FIGURE 1. Photograph of the shingle mini-module used in this work consisting of three solar cells (a), a schematic illustration of the shingle module as a top view indicating the ECA strips printed on the overlapping area (b) and a cross-sectional view of the encapsulated module displaying the PV module components used (c).

EXPERIMENTAL PART

Shingle Module Preparation

The shingled interconnected solar modules consist of three silicon cells (14.8 x 2.2 cm^2) arranged in a step-like configuration and connected in series by applying ECA. The ECA was screen printed onto the solar cells as eight strips with the same length according to [4] (Fig.1). The strips were applied at the interfaces between cells and between the front and back cells, and their respective interconnect ribbons. The shingle modules (20.0 x 20.0 cm^2) were prepared by laminating the silicon cells sandwiched between two layers of encapsulant material, a layer of transparent polymer-based backsheet foil (BS), and a transparent glass cover.

Scanning Acoustic Microscopy

The PV modules were laid flat into a water tank and scanned by a SAM HD² (PVA TePla Systems GmbH, Westhausen, Germany) using a 15 MHz transducer at ambient conditions. Acoustic micrographs from different depths were acquired to enable a detailed inspection of the inner structure of the module components and the ECA strips. The spatial resolution was set to 40 µm/pixel. Acoustic cross-sections of the PV modules were extracted to visualize the depth profile. The shingle modules were measured through the BS foil (see Fig. 1)

X-Ray Imaging

The analyzed shingle modules were imaged with a Dage XD7600NT X-ray microscope. The measurement is based on transmitted light, in which images are acquired based on the spatially varying absorption properties of the sample. The resulting contrast strongly depends on the absorption properties of the materials for Cu K_α radiation of 1.54 Å wavelength. The equipment provides a resolution limit down to 250 nm, besides enabling inspection from different angles. The images shown in this work were acquired at 120-140 kV acceleration voltage and 2.0 to 2.3 W power. The samples are examined through the glass.

Electroluminescence

The EL images were taken with a greateyes GE 1024 256 NIR CCD camera using a 50 mm lens. As irregularities in the ECA mainly result in series resistance losses, the images were taken at a current of 1 A, which is close to the I_{SC} of the shingled cells. The images were taken from the front side of the modules.

RESULTS

SAM enables imaging the whole area of the solar module at any desired depth. Figure 2 shows SAM images of a shingle module taken at different depths. Figure 2a depicts the backside of the cells at the encapsulant/cell interface. The black dots in the image are air bubbles within the encapsulant. Figure 2b was taken at a deeper level and it shows the eight ECA strips between the upper cell and the ribbon (red area). The ECA strips between the cells can be visualized in Fig. 2c. They appear dark and are well distinguished from the spots without ECA. Discontinuities present in the ECA strips can also be seen in Fig. 2b and c. The depth chosen for a given image is determined by the position and length of the gate applied during the measurement. The gates are indicated as green lines in Fig. 4.

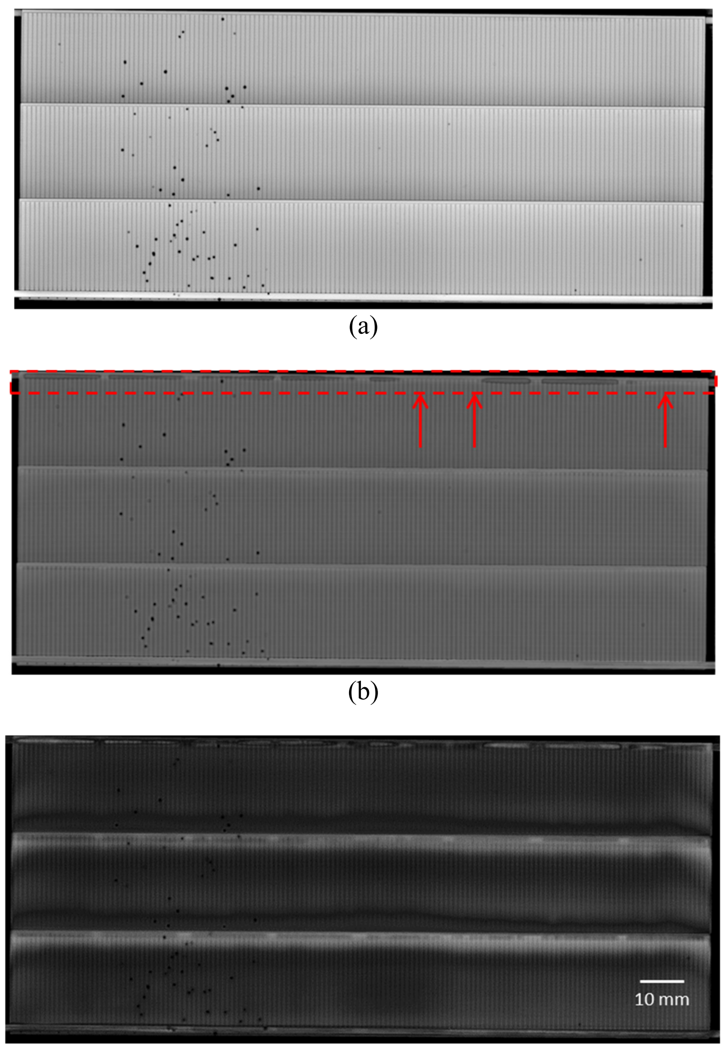

(a)

(b)

(c)

FIGURE 2. SAM images at different depths of shingle module: at the encapsulant/cell interface (a), upper cell/ECA interface (b) and on the cell/ECA interfaces between the cells (c). Spatial resolution: 40 µm/pixel.

In the SAM images shown in Fig. 2, the ECA is depicted dark because the echo reflected from the cell/ECA interfaces arrives at a lower amplitude at the transducer. Areas without ECA appear much brighter, and this indicates higher ultrasound reflection. Particularly, Fig. 2b shows that parts of the ECA strips are missing (indicated by arrows). The different reflection behaviors can be seen in the acoustic cross-section shown in Fig.3. It depicts a 2D time-domain visualization of the depth profile at the cross-section plane indicated by the red line. Since the SAM measurements were done from the BS towards the glass, the upper lines correspond to the wave reflections at the water/BS, BS/encapsulant, encapsulant/cell, and the cell/ECA interfaces. The latter is indicated by the red arrow. The contrast at the cell/ECA interface confirms the observations in Fig. 2. At the interface between cell and ECA, there is less acoustic wave reflection; therefore, the ECA strips appear dark. In the opposite case, a larger reflection of ultrasound occurs at cell interfaces lacking ECA, i.e., at the spaces between strips, or at defective ECA strips. Observe that the defective ECA strips in Fig. 2b shows an increased reflection in the acoustic cross-section in Fig. 3. Therefore, missing ECA strips will appear brighter in the image.

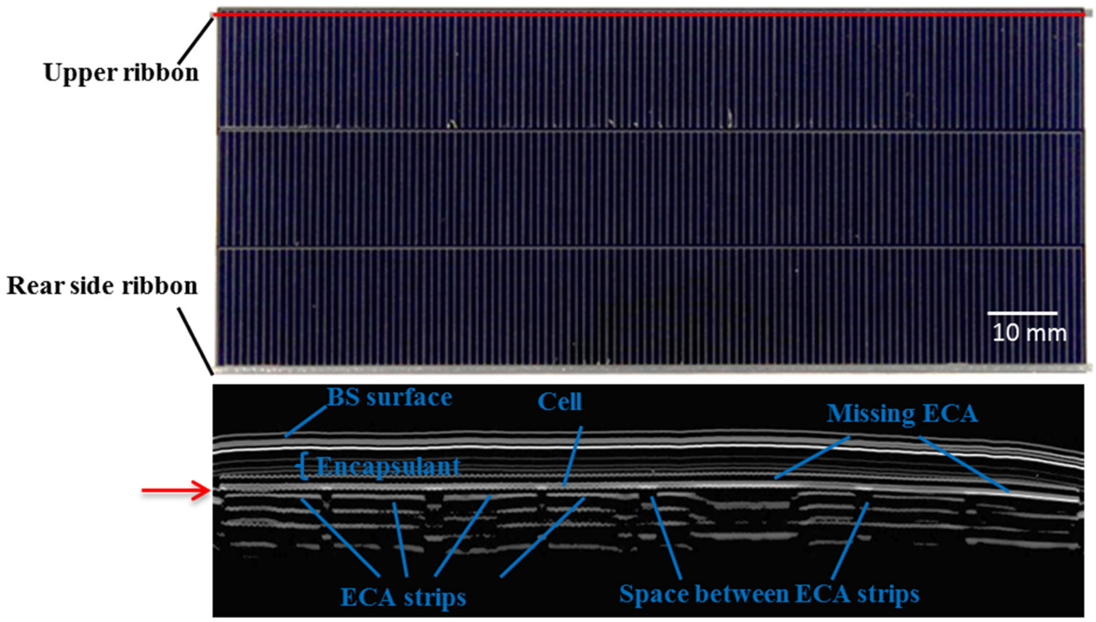

FIGURE 3. Photograph of a shingled solar module (top) and the corresponding acoustic cross-section (bottom) taken at the indicated red line. The red arrow shows the interface of interest. The bright regions are caused by reflection of the acoustic wave upon absence of ECA; x axis = 200 mm; y axis = TOF (µs).

This finding further reveals that the acoustic impedance mismatch at the interface between a solar cell and an ECA strip is lower than that in the absence of ECA. Therefore, the absence of ECA, even if partially, is detected by SAM. To illustrate this, we extracted the time-domain reflectograms of two different points on the solar cell along the upper ribbon: at a cell/ECA and cell/no ECA interface. The results are shown in Fig. 4. The amplitude of the echo measured by the transducer represents the signal magnitude, which reflects the acoustic mismatch of the materials at their interface. Therefore, the higher the signal magnitude, the brighter the contrast in the image will be.

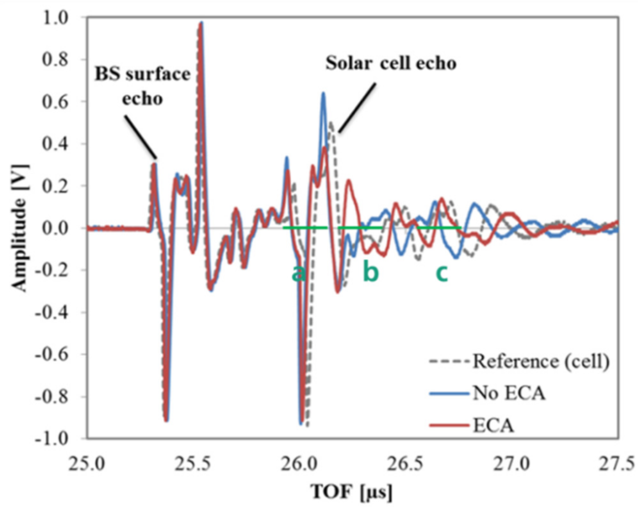

FIGURE 4. Time-domain reflectograms displaying the cell interface echo at a point with and without ECA (red and blue lines, respectively) between the upper cell and ribbon, and a reference cell echo (no ECA, not along a ribbon). The green lines indicate the interfaces at which the images in Fig. 2 were obtained: at the encapsulant/cell interface (a), cell/ECA interface on the back ribbon (b) and on the cell/ECA interfaces between the cells (c).

Fig. 4 shows that the amplitude of an echo from a cell/ECA interface is lower than that from an interface without ECA. That is, the impedance mismatch at an interface between the solar cell and ECA is lower. Therefore, less reflection occurs. In contrast, the higher mismatch at an interface without ECA results in higher ultrasound reflection. Hence, the spaces between the ECA strips appear brighter in the acoustic cross-section (Fig. 3). The lower impedance mismatch at an ECA-containing interface can be explained by the fact that the ultrasound is transmitted more from the top cell through a material with similar acoustic properties, i.e., the ECA. On the other hand, a high reflection occurs at an interface with a higher impedance mismatch, i.e., when ultrasound propagates from the cell to an interface void of material. A schematic illustration of the acoustic reflection behavior at the interfaces studied is shown in Fig. 5.

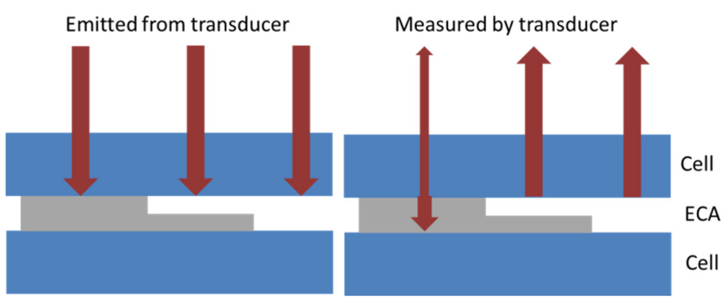

FIGURE 5. Schematic illustration of the transmission and reflection of the acoustic wave at the interfaces between the solar cell and ECA, and without ECA.

Therefore, this confirms the potential of SAM to visualizing defective ECA spots on shingled interconnected solar cells. Next, we compare SAM with X-ray images to assess the suitability of SAM as an alternative method for the qualitative analysis of the ECA joints in shingled modules. The results are shown in Fig.6.

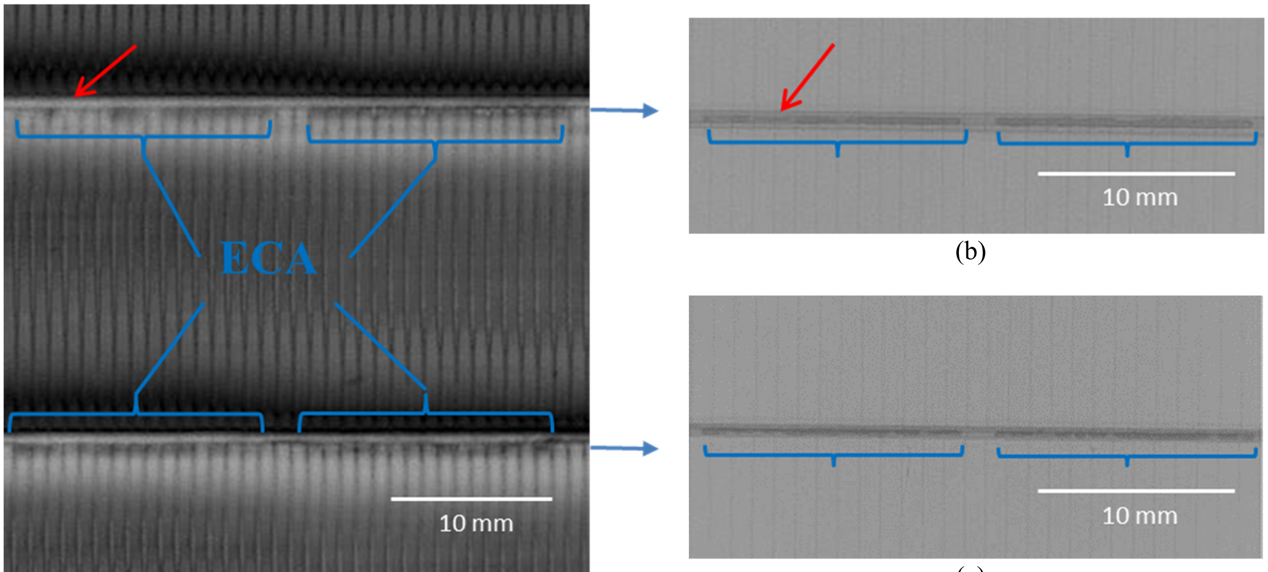

(a) (b) (c)

FIGURE 6. SAM (a) and X-ray images (b, c) of shingled modules displaying the ECA between the solar cells.

Figure 6 shows SAM and X-ray images of the same area of the shingled module. Both images show good agreement in displaying the ECA strips. The screen-printed silver fingers and ECA strips appear dark in the X-ray images. The visible ECA strips are between two shingled cells. The images show that the ECA is irregular across the strips, besides noticeable flaws. The red arrows indicate a region where irregularities on the ECA structure are visualized in both techniques. While this defect is immediately detected in the SAM image, the X-ray image reveals only a subtle contrast loss, which suggests local variations in ECA quantity. This further indicates that, despite the presence of ECA at the interface, the latter may not have fully adhered to the cell, hence the higher reflection at the interface. Therefore, this shows how SAM is a complementary technique on the interpretation of the results.

There is, however, a discrepancy regarding the resolution of the images. The X-ray image has a better resolution than SAM such that the ECA strips are clearer to distinguish. In the SAM image, the ECA contours appear blurred and larger, and the silver fingers appear much thicker. This is explained by the tradeoff between ultrasound penetration and resolution. Because the resolution in a microscope depends on the wavelength and the frequency [1], the ultrasound frequency used in this work (15 MHz) might have resulted in a resolution loss. That means that a higher frequency would improve the resolution, but decrease the ultrasound penetration [9]. That means that the SAM images at this may provide only an approximate estimate of the ECA real dimensions.

After imaging the shingled modules with SAM and X-ray, we attempt to assess the influence of the structural failure of the ECA strips on the electrical properties of the shingled module. The EL image of the module (Fig. 7a) shows large inhomogeneity across the cells. As the ECA strips are equally applied at each cell, the transport of electrons should be equally distributed, and the EL intensity should be homogeneous throughout the cell area. In the area A1, there is a higher current density across the cells. In the area A2, the EL image reveals poor electron mobility. There, it is expected that some ECA strips might be defective. In Fig. 7b the SAM image can be directly compared with the EL image. In order to visualize possible defective ECA strips, SAM and X-ray images of A1 and A2 are compared. These are shown in Fig. 8.

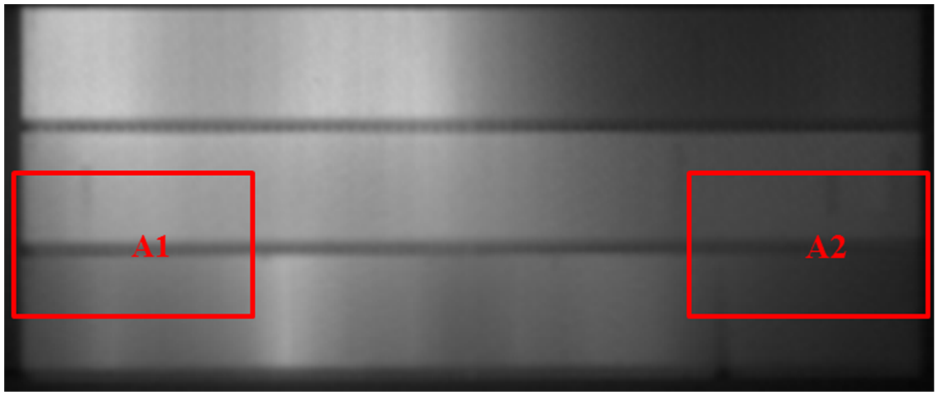

(a)

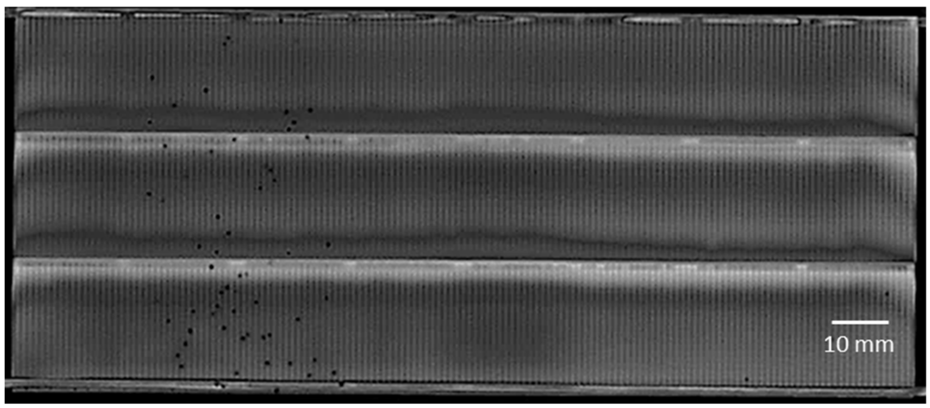

(b)

FIGURE 7. EL (a) and SAM (b) images of the shingled module. Detailed images of the areas A1 and A2 are shown in Fig. 8.

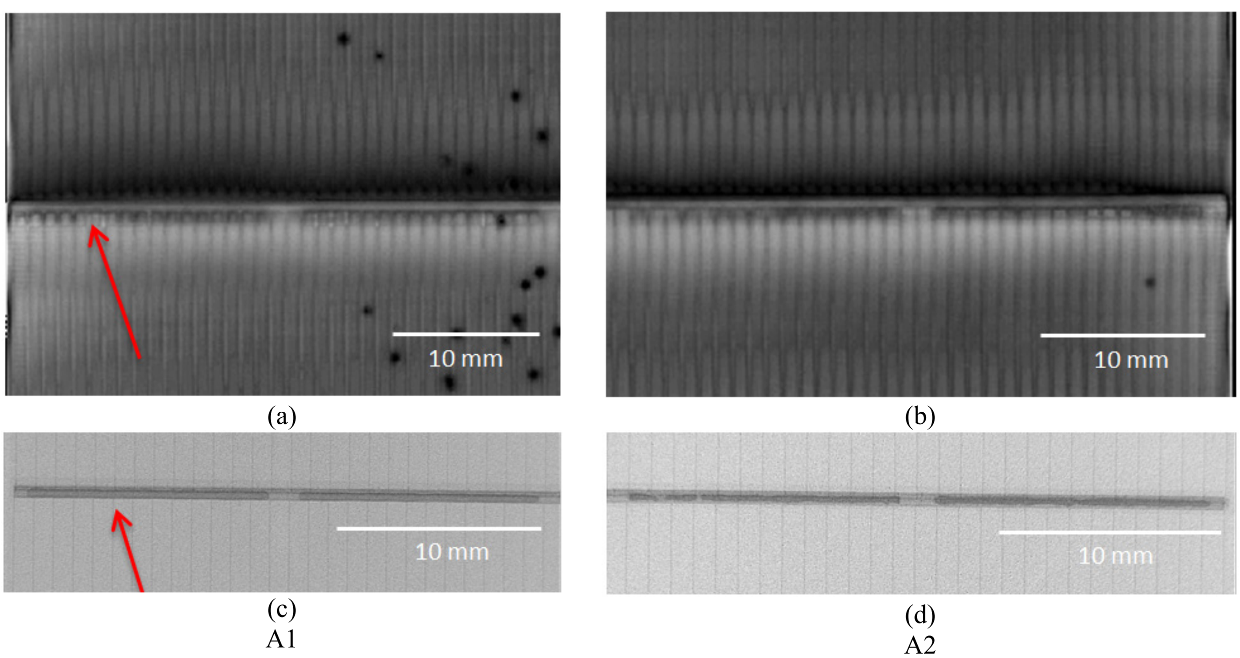

FIGURE 8. SAM (a, b) and X-ray (c, d) images of A1 (a, c) and A2 (b, d).

Figure 8 shows that the ECA strips can be distinguished in both techniques, although the ECA contrast in the SAM images is not so easy to interpret. Nevertheless, ECA irregularities can be detected in both images in the area A2, which might explain the poor electrical performance in this region (see Fig.7a) to some extent. In the area A1, the X-ray image shows that the ECA looks homogeneous and intact (Fig. 8c). The SAM image reveals, however, a bright spot (red arrow) along an ECA strip, which does not match exactly to the pattern observed in the corresponding X-ray image. Therefore, we assume that an ECA strip that looks physically well distributed and intact, as evidenced by the X-ray imaging, might be nevertheless poorly connecting two adjacent cells. Furthermore, a direct correlation between defective ECA strips with the EL intensity could not be observed because we assume that other ECA joints performing poorly are likely present. However, these issues are subject to future investigations. Moreover, an improved choice of parameters for the SAM analysis, for example, the ultrasound frequency could result in a finer resolution, thus increasing the detection limit. Therefore, despite this limitation, we have shown that SAM is an alternative technique to investigate the distribution of ECA in shingled modules.

CONCLUSION

Because ultrasound is sensitive to interfaces with different acoustic impedances, it makes SAM a powerful candidate for the non-destructive analysis of ECA joints in shingled interconnected solar cells. We have compared SAM images with X-ray images and demonstrated that both techniques are in agreement in displaying the distribution of ECA strips, as well as irregularities. There are, however, advantages in using SAM, particularly the possibility of generating acoustic cross-sections, as well as images from individual depths. The acoustic cross-section presented in this work showed the internal arrangement of the solar module and the distinction between defective and intact ECA strips. Furthermore, SAM enables imaging solar modules of different sizes, including full-size modules. In contrast, the X-ray chamber has a limited size, and the analysis of larger modules is not possible. The future outlook is to quantify defective ECA areas with SAM based on the images and the received signal.

ACKNOWLEDGMENTS

We thank Sandor Stecklum for the support in interpreting the EL images.

REFERENCES

1. A. Briggs, Reports on Progress in Physics **55**, 851–909 (1992).
2. S. Brand, S. Tismer, S. T. Moe and K. Schjølberg-Henriksen, Microsystem Technologies **21**, 1385–1394 (2015).
3. P. Baliozian, E. Lohmüller, T. Fellmeth, N. Wöhrle, A. Krieg, and R. Preu, *Sol. RRL* 1700171, 1-5 (2018).
4. A. Mondon, N. Klasen, E. Fokuhl, M. Mittag, M. Heinrich, and H. Wirth, "Comparison of layouts for shingled bifacial PV modules in terms of power output, cell-to-module ratio and bifaciality". Proceedings of the 35th European PV Solar Energy Conference and Exhibition, (2018).
5. N. Klasen, A. Mondon, A. Kraft and U. Eitner, "Shingled Cell Interconnection: A New Generation of Bifacial PV-Modules", 7th Workshop on Metallization and Interconnection for Crystalline Silicon Solar Cells (2017).
6. T. Geipel, L. C. Rendler, M. Stompe, U. Eitner and L. Rissing, Energy Procedia *77*, 346 – 355 (2015).
7. B. King, D. Moore, O. Lavrova, "Non-destructive Evaluation of Full-size Photovoltaic Modules", DuraMat Workshop (2016).
8. R. Hanke, T. Fuchs, N. Uhlmann, "X-ray based methods for non-destructive testing and material characterization", Proceedings of the 9th International Workshop on Radiation Imaging Detectors **591**, 14-18 (2008).
9. R.G. Maev, M.P. Pyshnyi, E.Yu. Maeva, K.I. Maslov and V.M. Levin. Review of Progress in Quantitative Nondestructive Evaluation **16**, 1845-1851 (1997).